Journal of Materials Chemistry A

RSC Publishing

PAPER

View Article Online
View Journal | View Issue

# $Ag_{0.1}$-$Pd_{0.9}$/rGO: an efficient catalyst for hydrogen generation from formic acid/sodium formate†

**Cite this:** *J. Mater. Chem. A*, 2013, **1**, 12188

Received 14th July 2013
Accepted 7th August 2013

DOI: 10.1039/c3ta12724a

**www.rsc.org/MaterialsA**

Yun Ping, Jun-Min Yan,* Zhi-Li Wang, Hong-Li Wang and Qing Jiang

$Ag_{0.1}Pd_{0.9}$ nanoparticles assembled on reduced graphene oxide are synthesized by a facile co-reduction route. The resultant AgPd nanoparticles/reduced graphene oxide exert 100% $H_2$ selectivity and exceedingly high activity toward the complete decomposition of formic acid at room temperature under ambient conditions.



Hydrogen ($H_2$), which is widely accepted as a promising energy carrier for transport/mobile applications may play an important role in renewable energy technologies in the future.[1] However, due to the extremely low critical point and very low density of $H_2$ gas, efficient storage of $H_2$ remains a bottleneck for the $H_2$ based fuel cell economy.[2,3] As an alternative, chemical $H_2$ storage has been attracting considerable attention. Formic acid (FA, HCOOH), one of the major products formed in biomass processing, is nontoxic and highly stable with a high $H_2$ content (4.4%)[4] at room temperature, making it a safe and convenient $H_2$ carrier in fuel cells for portable use.[5] FA can be decomposed to $H_2$ and $CO_2$ *via* a dehydrogenation pathway ($HCOOH(l) \rightarrow H_2(g)+CO_2(g)$, $\Delta G_{298K} = -35.0$ kJ mol$^{-1}$)[6–8] in the presence of a suitable catalyst. However, the undesirable dehydration pathway ($HCOOH(l) \rightarrow H_2O(l)+CO(g)$, $\Delta G_{298K} = -14.9$ kJ mol$^{-1}$)[9–11] to generate carbon monoxide (CO), which is a fatal poison to catalysts in fuel cells, should be avoided by adjusting the catalysts, pH values of the solutions, as well as the reaction temperatures.[12]

Metallic particles with ultrafine sizes have attracted tremendous research interest because of their unique catalytic properties compared to their bulk counterparts due to the high surface area and the number of edge and corner atoms.[13] However, small particles, especially on the nanoscale, are frequently subjected to the problem of aggregation, resulting from their high surface energy,[14] which usually leads to the serious reduction of their catalytic properties. To avoid this issue, various types of support materials have been employed to uniformly disperse the nanoparticles (NPs).[15,16] Graphene, a single-layer carbon material,[17] attracts tremendous attention owing to its high conductivity ($10^3$–$10^4$ S m$^{-1}$), huge theoretical surface area (2600 m$^2$ g$^{-1}$), unique graphitized basal plane structure, and potentially low manufacturing costs.[18] With these advantages, graphene-based nanomaterials are being explore for use in sensors,[19] electronics,[20] electrochemical energy storage,[21] efficient catalysts,[22] *etc.* In catalytic studies, its close contact with metal NPs is believed to play a significant role in the activity enhancement of the catalyst.[13,23] Thus, graphene is a promising candidate as an ideal substrate to anchor various functional groups with accessible active sites for high performance catalysis.[24–27]

Herein, a facile co-reduction route is successfully utilized to synthesize $Ag_{0.1}Pd_{0.9}$ NPs assembled on reduced graphene oxide ($Ag_{0.1}Pd_{0.9}$/rGO), wherein the rGO plays a key role as a powerful dispersion agent and distinct support for the $Ag_{0.1}Pd_{0.9}$ NPs. The resultant $Ag_{0.1}Pd_{0.9}$/rGO hybrid exerts 100% $H_2$ selectivity and exceedingly high activity toward the complete decomposition of FA at room temperature under ambient conditions.

Graphene oxide (GO) dispersed in water is firstly prepared using the modified Hummers' method as the graphene precursor.[28] The $Ag_{0.1}Pd_{0.9}$/rGO hybrid is synthesized by co-reduction of GO and the metal precursors of Ag and Pd, as shown in Fig. 1. Typically, $Ag_{0.1}Pd_{0.9}$/rGO is prepared by dispersing GO (3 mL, 10.9 mg mL$^{-1}$) into 10 mL of water with ultrasonication for 40 min. Then, 5.0 mL of aqueous solution containing $AgNO_3$ (0.01 mM), $Na_2PdCl_4$ (0.09 mM) is added into the above suspension with magnetic stirring for 30 min.

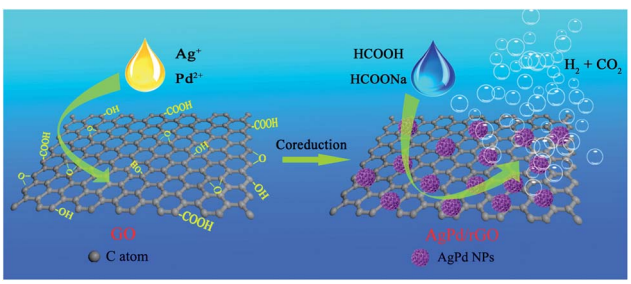


**Fig. 1** Schematic illustration for preparation of AgPd/rGO.

*Key Laboratory of Automobile Materials Ministry of Education, Department of Materials Science and Engineering, Jilin University, Changchun 130022, China. E-mail: junminyan@jlu.edu.cn*

† Electronic supplementary information (ESI) available. See DOI: 10.1039/c3ta12724a

Subsequently, the above mixture is reduced by a freshly prepared aqueous solution of $NaBH_4$ (1.05 M, 1.0 mL). After 2 h, the obtained product is washed with water several times and re-dispersed in 10 mL of water for the catalytic $H_2$ generation from the FA aqueous solution at 298 K.

The morphologies of the as-prepared $Ag_{0.1}Pd_{0.9}$/rGO hybrid and free $Ag_{0.1}Pd_{0.9}$ NPs are characterized by transmission electron microscopy (TEM). It can be seen that the as-synthesized $Ag_{0.1}Pd_{0.9}$ with GO are uniformly dispersed on rGO with an average particle size of about 6 nm (Fig. 2a and b), while the NPs prepared without GO are severely aggregated (Fig. 2d), indicating that rGO lead to the good dispersion of $Ag_{0.1}Pd_{0.9}$ NPs on its surface. It is widely believed that oxygen-containing functionalities in GO, such as carboxylic (–COOH), carbonyl (–C=O), and hydroxy (–OH) groups, are necessary for anchoring metal ions,[29] which thus help to control the sizes and distributions of the formed metal NPs on the rGO during the synthetic process.[30] The high resolution TEM (HRTEM) image (Fig. 2c) reveals the crystalline nature of the $Ag_{0.1}Pd_{0.9}$ NPs, and the lattice spacing is measured to be 0.230 nm, which is between the (111) plane of face-centered cubic (fcc) Ag (0.235 nm)[31] and fcc Pd (0.224 nm).[32] The X-ray diffraction (XRD) pattern of the $Ag_{0.1}Pd_{0.9}$/rGO hybrid and free $Ag_{0.1}Pd_{0.9}$ (Fig. 3a) show that the diffraction peaks are located between peaks expected from pure Pd (JCPDS: 46-1043)[33] and Ag (JCPDS: 04-0783),[33] strongly indicating the formation of an alloyed structure. In addition, there is only one sharp peak centered at $2\theta = 9.72°$ in the XRD pattern of the GO (Fig. S1†), corresponding to a distance of 9.092 Å between the stacked GO sheets. After reduction, the GO peak disappeared from the XRD pattern and a broad peak around 25° emerged, indicating that GO has been reduced to rGO.[34] Based on the above results, the $Ag_{0.1}Pd_{0.9}$ NPs with an alloy structure supported on rGO have been successfully synthesized by the present method.

X-Ray photoelectron spectroscopy (XPS) measurements are performed to determine the compositions and chemical states

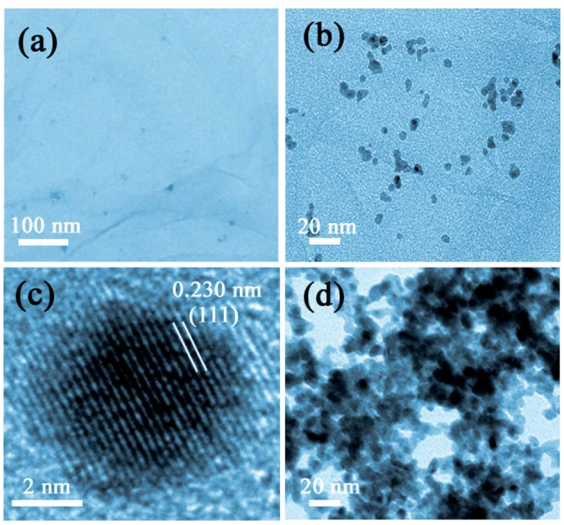


**Fig. 2** TEM images with the (a) low, (b) middle and (c) high resolution for $Ag_{0.1}Pd_{0.9}$/rGO hybrid, and (d) TEM image for free $Ag_{0.1}Pd_{0.9}$ NPs.

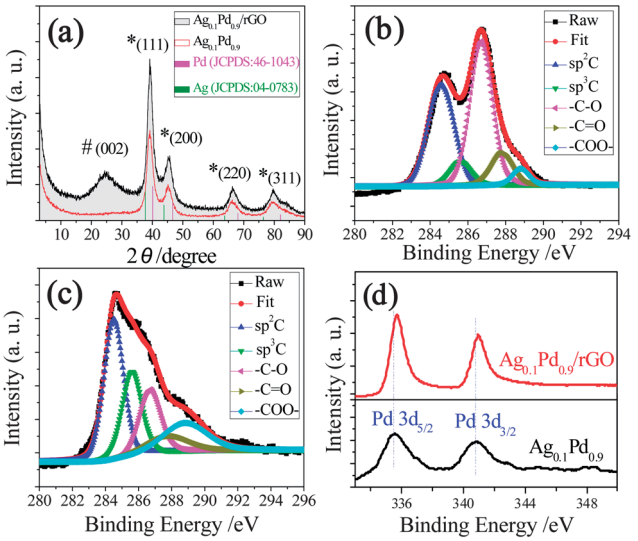


**Fig. 3** XRD pattern of (a) $Ag_{0.1}Pd_{0.9}$/rGO and free $Ag_{0.1}Pd_{0.9}$ NPs: *AgPd alloy, # rGO, the C 1s peaks in the XPS spectra of (b) GO and (c) $Ag_{0.1}Pd_{0.9}$/rGO, XPS spectra of Pd 3d for (d) the free $Ag_{0.1}Pd_{0.9}$ and $Ag_{0.1}Pd_{0.9}$/rGO.

of the $Ag_{0.1}Pd_{0.9}$/rGO hybrid. The result for C 1s of the as-prepared GO (Fig. 3b) indicates that five different peaks centered at 284.5, 285.6, 286.7, 287.8 and 288.8 eV are observed, corresponding to $sp^2C$, $sp^3C$, –C–O, –C=O and –COO groups, respectively.[35] However, after reduction, the intensities of all the C 1s peaks binding to oxygen obviously decrease (Fig. 3c), revealing that most of the oxygen containing species are removed and the majority of the conjugated C networks are restored. This confirms the reduction of GO to rGO during the preparation of the $Ag_{0.1}Pd_{0.9}$/rGO hybrid, which is consistent with the Raman (Fig. S2†) and ultraviolet visible (UV-Vis, Fig. S3†) spectra. On the other hand, elements of Pd and Ag in the final product are in their metallic states (Fig. 3d, and S4†).[36,37] Moreover, the binding energies of Pd 3d in the $Ag_{0.1}Pd_{0.9}$/rGO hybrid shift slightly relative to that in free $Ag_{0.1}Pd_{0.9}$ NPs (Fig. 3d), implying that rGO interacts strongly with the metal NPs. Such interaction may be one of the promotion effects for the efficient decomposition of FA.

The catalytic activities of the as-prepared $Ag_{0.1}Pd_{0.9}$/rGO hybrid, together with the free $Ag_{0.1}Pd_{0.9}$ NPs and rGO for $H_2$ generation from FA decomposition at 298 K under ambient atmosphere are presented in Fig. 4. It should be noted that only the mixture of $H_2$ and $CO_2$ but no CO (detection limit: ~10 ppm for CO) has been detected by gas chromatography (GC) analyses (Fig. S5 and S6†), which means that the present $Ag_{0.1}Pd_{0.9}$/rGO hybrid has an excellent $H_2$ selectivity for FA dehydrogenation. Finally, 303 mL of gas, a large volume far exceeding the theoretical value from FA dehydrogenation (244 mL), can be generated within 120 min at 298 K. Thereby, the excess of gas is contributed to $H_2$ generated from hydrolysis of sodium formate (SF) in this system.[11] Considering the gas generated from the present FA/SF system, the theoretical molar ratio of $H_2 : CO_2$ should be 1.66 : 1. However, the measured value by GC is 1.44 : 1. This may result from the small levels of $CO_2$ from

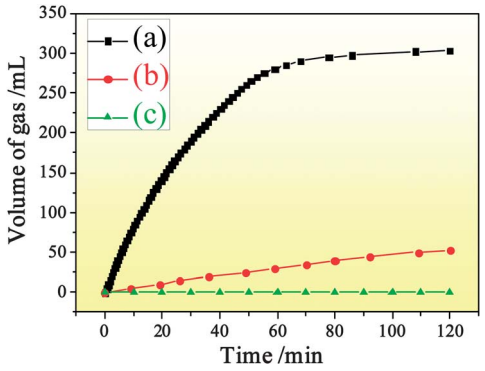


**Fig. 4** Gas generation by the decomposition of FA/SF (1 M/0.67 M, 5 mL) *vs.* time in the presence of (a) $Ag_{0.1}Pd_{0.9}$/rGO hybrid, (b) free $Ag_{0.1}Pd_{0.9}$ NPs, (c) rGO at 298 K under ambient atmosphere ($n_{AgPd}/n_{FA} = 0.02$).



$NaHCO_3$ in the present acid solution.[11] Based on the volume of $H_2$ (179 mL), the total conversion for the decomposition of the FA/SF system can reach the value of 87.8% within 120 min. Furthermore the turnover frequency (TOF) is calculated to be 105.2 mol $H_2$ $mol^{-1}$. catalyst. $h^{-1}$ at 298 K after 20 min, which is faster than that of the most active catalysts ever reported at the room temperature (ESI Table S1†).[6,8,10,11,38] On the other hand, without rGO, the free $Ag_{0.1}Pd_{0.9}$ NPs exhibit much lower activity than that of $Ag_{0.1}Pd_{0.9}$/rGO hybrid, and only 45 mL of gas is obtained after 120 min (Fig. 4b), suggesting that rGO plays a key role in the decomposition of FA/SF. To further investigate if rGO has a dramatic effect on the $Ag_{0.1}Pd_{0.9}$/rGO hybrid, the catalytic activity of the physical mixture of $Ag_{0.1}Pd_{0.9}$ and rGO is also examined. As a result, the physical mixture shows much lower activity than that of the $Ag_{0.1}Pd_{0.9}$/rGO hybrid under analogous conditions (Fig. S7†). Reasonably, the superior catalytic performance of the $Ag_{0.1}Pd_{0.9}$/rGO hybrid may be attributed to the synergistic coupling between $Ag_{0.1}Pd_{0.9}$ and rGO, which results from the rGO microstructure, including the defects, types and surface densities of oxygen-containing functionalities.[39] Assisted by the favorable microstructure, rGO can lead to a strong metal-support interaction and resultant resistance of NPs to aggregation, thus efficiently increasing the $H_2$ generation rate for the decomposition of FA.

To determine the effect of the metal composition in AgPd/rGO on the catalytic performance, the molar ratio of Ag : Pd has been varied. As a result, the best one is 0.1 : 0.9 for Ag : Pd (Fig. S8†).

It is noteworthy that, the molar ratio of FA to SF has an obvious effect on the performance of the resulting $Ag_{0.1}Pd_{0.9}$/rGO hybrid (Fig. S9†). When the molar percent of FA is increased from the present value of 60% (75%, 100%), the activity of the $Ag_{0.1}Pd_{0.9}$/rGO hybrid decreases (Fig. S9a and b†). On the other hand, when the molar percent of FA is decreased to 50%, the activity of the catalyst shows no obvious change (Fig. S9d†). However, without FA, no gas can be generated over the same catalyst (Fig. S9e†).

In summary, $Ag_{0.1}Pd_{0.9}$ NPs decorated on rGO are successfully synthesized by co-reduction of GO and the metal precursors. The resultant $Ag_{0.1}Pd_{0.9}$/rGO hybrid serves as a highly efficient catalyst to facilitate the liberation of CO-free $H_2$ from FA/SF aqueous solution at room temperature. This improvement in the catalytic performance of the new $Ag_{0.1}Pd_{0.9}$/rGO composite may further promote the practical application of FA as a $H_2$ storage material.

## Acknowledgements

This work is supported in part by National Key Basic Research, Development Program (2010CB631001); National Natural Science Foundation of China (51101070) Program for Changjiang Scholars and Innovative Research Team in University; Program for New Century Excellent Talents in University of the Ministry of Education of China (NCET-09-0431); Jilin Province Science and Technology Development Program (201101061); and Jilin University Fundamental Research Funds.

## References

1 T. M. McCormick, B. D. Calitree, A. Orchard, N. D. Kraut, F. V. Bright, M. R. Detty and R. Eisenberg, *J. Am. Chem. Soc.*, 2010, **132**, 15480–15483.
2 J. M. Yan, X. B. Zhang, S. Han, H. Shioyama and Q. Xu, *Angew. Chem., Int. Ed.*, 2008, **47**, 2287–2289.
3 X. B. Zhang, J. M. Yan, S. Han, H. Shioyama and Q. Xu, *J. Am. Chem. Soc.*, 2009, **131**, 2778–2779.
4 K. Mori, M. Dojo and H. Yamashita, *ACS Catal.*, 2013, **3**, 1114–1119.
5 H. L. Jiang, S. K. Singh, J. M. Yan, X. B. Zhang and Q. Xu, *ChemSusChem*, 2010, **3**, 541–459.
6 K. Tedsree, T. Li, S. Jones, C. W. A. Chan, K. M. K. Yu, P. A. J. Bagot, E. A. Marquis, G. D. W. Smith and S. C. E. Tsang, *Nat. Nanotechnol.*, 2011, **6**, 302–307.
7 S. Enthaler and B. Loges, *ChemCatChem*, 2012, **4**, 323–325.
8 Z. L. Wang, J. M. Yan, Y. Ping, H. L. Wang, W. T. Zheng and Q. Jiang, *Angew. Chem., Int. Ed.*, 2013, **52**, 4406–4409.
9 S. Zhang, Ö. Metin, D. Sun and S. Sun, *Angew. Chem., Int. Ed.*, 2013, **52**, 3681–3684.
10 Q. Y. Bi, X. L. Du, Y. M. Liu, Y. Cao, H. Y. He and K. N. Fan, *J. Am. Chem. Soc.*, 2012, **134**, 8926–8933.
11 Z. L. Wang, J. M. Yan, H. L. Wang, Y. Ping and Q. Jiang, *Sci. Rep.*, 2012, **2**, 598.
12 S. Fukuzumi, T. Kobayashi and T. Suenobu, *J. Am. Chem. Soc.*, 2010, **132**, 1496–1497.
13 X. Chen, G. Wu, J. Chen, X. Chen, Z. Xie and X. Wang, *J. Am. Chem. Soc.*, 2011, **133**, 3693–3695.
14 R. J. White, R. Luque, V. L. Budarin, J. H. Clark and D. J. Macquarrie, *Chem. Soc. Rev.*, 2009, **38**, 481–494.
15 X. Gu, Z. H. Lu, H. L. Jiang, T. Akita and Q. Xu, *J. Am. Chem. Soc.*, 2011, **133**, 11822–11825.
16 M. Yadav, A. K. Singh, N. Tsumori and Q. Xu, *J. Mater. Chem.*, 2012, **22**, 19146–19150.
17 S. Guo and S. Sun, *J. Am. Chem. Soc.*, 2012, **134**, 2492–2495.
18 A. K. Geim and K. S. Novoselov, *Nat. Mater.*, 2007, **6**, 183–197.
19 C. Zhu, S. Guo, Y. Fang and S. Dong, *ACS Nano*, 2010, **4**, 2429–2437.

20 L. Britnell, R. V. Gorbachev, R. Jalil, B. D. Belle, F. Schedin, A. Mishchenko, T. Georgiou, M. I. Katsnelson, L. Eaves, S. V. Morozov, N. M. R. Peres, J. Leist, A. K. Geim, K. S. Novoselov and L. A. Ponomarenko, *Science*, 2012, **335**, 947–950.
21 X. Zhu, Y. Zhu, S. Murali, M. D. Stoller and R. S. Ruoff, *ACS Nano*, 2011, **5**, 3333–3338.
22 H. Zhang, X. J. Lv, Y. M. Li, Y. Wang and J. H. Li, *ACS Nano*, 2010, **4**, 380–386.
23 Y. Li, H. Wang, L. Xie, Y. Liang, G. Hong and H. Dai, *J. Am. Chem. Soc.*, 2011, **133**, 7296–7299.
24 X. Zhou, L. J. Wan and Y. G. Guo, *Adv. Mater.*, 2013, **25**, 2152–2157.
25 N. G. Sahoo, Y. Pan, L. Li and S. H. Chan, *Adv. Mater.*, 2012, **24**, 4203–4210.
26 X. Zhang, X. Chen, K. Zhang, S. Pang, X. Zhou, H. Xu, S. Dong, P. Han, Z. Zhang, C. Zhang and G. Cui, *J. Mater. Chem. A*, 2013, **1**, 3340–3346.
27 S. Zhu, C. Zhu, J. Ma, Q. Meng, Z. Guo, Z. Yu, T. Lu, Y. Li, D. Zhang and W. M. Lau, *RSC Adv.*, 2013, **3**, 6141–6146.
28 D. C. Marcano, D. V. Kosynkin, J. M. Berlin, A. Sinitskii, Z. Sun, A. Slesarev, L. B. Alemany, W. Lu and J. M. Tour, *ACS Nano*, 2010, **4**, 4806–4814.
29 X. Yan, Q. Li and L. S. Li, *J. Am. Chem. Soc.*, 2012, **134**, 16095–16098.
30 J. Wang, X. B. Zhang, Z. L. Wang, L. M. Wang and Y. Zhang, *Energy Environ. Sci.*, 2012, **5**, 6885–6888.
31 J. Yang, R. C. Dennis and D. K. Sardar, *Mater. Res. Bull.*, 2011, **46**, 1080–1084.
32 Y. Xiong, J. M. Mclellan, Y. Yin and Y. Xia, *Angew. Chem., Int. Ed.*, 2007, **46**, 790–794.
33 M. Liu, Y. Lu and W. Chen, *Adv. Funct. Mater.*, 2013, **23**, 1289–1296.
34 S. Sharma, A. Ganguly, P. Papakonstantinou, X. Miao, M. Li, J. L. Hutchison, M. Delichatsios and S. Ukleja, *J. Phys. Chem. C*, 2010, **114**, 19459–19466.
35 Z. J. Fan, W. Kai, J. Yan, T. Wei, L. J. Zhi, J. Feng, Y. M. Ren, L. P. Song and F. Wei, *ACS Nano*, 2011, **5**, 191–198.
36 H. Huang and X. Wang, *J. Mater. Chem.*, 2012, **22**, 22533–22541.
37 X. Wang, Y. Tang, Z. Chen and T. T. Lim, *J. Mater. Chem.*, 2012, **22**, 23149–23158.
38 S. Jones, J. Qu, K. Tedsree, X. Q. Gong and S. C. E. Tsang, *Angew. Chem., Int. Ed.*, 2012, **51**, 11275–11278.
39 W. Qin and X. Li, *J. Phys. Chem. C*, 2010, **114**, 19009–19015.